CHEMISTRY OF MATERIALS
Article

Chem. Mater. **2009,** *21,* 3183–3190 3183
DOI:10.1021/cm900663t

Synthesis and Characterization of Monodisperse Manganese Oxide Nanoparticles−Evaluation of the Nucleation and Growth Mechanism

Thomas D. Schladt, Tanja Graf, and Wolfgang Tremel*

Institut für Anorganische Chemie und Analytische Chemie, Johannes Gutenberg Universität Mainz, 55099 Mainz, Germany

Received March 8, 2009. Revised Manuscript Received June 15, 2009

Magnetic nanoparticles of the 3d transition metal oxides have gained enormous interest for applications in various fields such as data storage devices, catalysis, drug-delivery, and biomedical imaging. One major requirement for these applications is a narrow size distribution of the particles. We have studied the nucleation and growth mechanism for the formation of MnO nanoparticles synthesized by decomposition of a manganese oleate complex in high boiling nonpolar solvents using TEM, FT-IR, and AAS analysis. The exceptionally narrow size distribution indicates that nucleation and growth are clearly separated. This leads to a uniform growth with a very narrow size distribution on the existing nuclei. The particle size can be controlled by adjusting the reaction time, reaction temperature, solvent, and heating rate. The particle size increases with temperature, reaction time, and the chain length (boiling point) of the solvent. FT-IR and NMR spectra revealed that the oleate capping agent binds to the surface in a bidentate manner. In addition, XPS measurements indicate that MnO nanocrystals are air-stable. No significant oxidation of Mn^{2+} to Mn^{3+} occurred even after several days.

Introduction

Magnetic nanoparticles of the 3d transition metal oxides have gained enormous interest for applications in various fields such as data storage devices, catalysis, drug delivery, and biomedical imaging.[1−5] Especially nanocrystals of simple binary metal oxides like MnO, NiO, or CoO have served as model systems for the detailed description of magnetic properties in the nanometer regime.[6−8] Different from the antiferromagnetic bulk material, MnO exhibits ferromagnetic behavior when the crystallite size is decreased to a few nanometers. Multiple attempts have been made to explain this behavior. The common opinion today is based on the presence of uncompensated spins on the crystal surface.[9]

Over the past years, several different synthesis methods have been developed to produce magnetic nanoparticles in various sizes and shapes. However, one major requirement concerning later application in the above-mentioned areas is a narrow size distribution of the particles, usually with $\sigma < 10\%$. On the basis of the La Mer model,[10] a separation of nucleation and growth is necessary in order to achieve such a narrow size distribution. Therefore, a detailed knowledge of the nucleation and growth process is essential. A commonly used approach is the "hot-injection" method in which a cold precursor is injected into a hot solvent. The fast increase in monomer concentration leads to a short nucleation event. Both concentration and temperature rapidly decrease, followed by a simultaneous growth of all particles as the precursor concentration is depleted.

During the last years many "one-pot" methods have been developed for the synthesis of monodisperse nanoparticles in which all components are heated at the same time. MnO nanoparticles have been synthesized starting from $Mn_2(CO)_8$,[11] manganese acetylacetonate,[12] acetate,[13] or formate[14] in trioctylamine, with oleic acid as a stabilizing agent and manganese cupferronate[8] complexes or fatty acid salts in high boiling solvents.[15] Most of these methods use oleic acid as a surfactant to control nucleation and growth and it must be expected that a

*Corresponding author. Phone: 49 6131 392-5135. Fax: 49 6131 392-5605. E-mail: tremel@uni-mainz.de.

(1) Raj, K.; Moskowitz, R. *J. Magn. Magn. Mater.* **1990**, *85*, 233–245.
(2) Sun, S.; Murray, C. B.; Weller, D.; Folks, L.; Moser, A. *Science* **2000**, *287*, 1989–1992.
(3) Hyeon, T. *Chem. Commun.* **2003**, 927–934.
(4) Sun, S. *Adv. Mater.* **2006**, *18*, 393–403.
(5) Jun, Y.-W.; Lee, J.-H.; Cheon, J. *Angew. Chem., Int. Ed.* **2008**, *47*, 5122–5135.
(6) Kodama, R. H. *J. Magn. Magn. Mater.* **1999**, *200*, 359–372.
(7) Makhlouf, S. A.; Parker, F. T.; Spada, F. E.; Berkowitz, A. E. *J. Appl. Phys.* **1997**, *81*, 5561–5563.
(8) Ghosh, M.; Biswas, K.; Sundaresan, A.; Rao, C. N. R. *J. Mater. Chem.* **2006**, *16*, 106–111.
(9) Kodama, R. H.; Makhlouf, S. A.; Berkowitz, A. E. *Phys. Rev. Lett.* **1997**, *79*, 1393–1396.
(10) LaMer, V. K.; Dinegar, R. H. *J. Am. Chem. Soc.* **1950**, *72*, 4847–4854.
(11) Lee, G. H.; Huh, S. H.; Jeong, J. W.; Choi, B. J.; Kim, S. H.; Ri, H.-C. *J. Am. Chem. Soc.* **2002**, *124*, 12094–12095.
(12) Seo, W. S.; Jo, H. H.; Lee, K.; Kim, B.; Oh, S. J.; Park, J. T. *Angew. Chem., Int. Ed.* **2004**, *43*, 1115–1118.
(13) Yin, M.; O'Brien, S. *J. Am. Chem. Soc.* **2003**, *125*, 10180–10181.
(14) Zhong, X.; Xie, R.; Sun, L.; Lieberwirth, I.; Knoll, W. *J. Phys. Chem. B* **2006**, *110*, 2–4.
(15) Park, J.; An, K.; Hwang, Y.; Park, J. G.; Noh, H. J.; Kim, J. Y.; Park, J. H.; Hwang, N. M.; Hyeon, T. *Nat. Mater.* **2004**, *3*, 891–895.

Published on Web 07/06/2009

metal oleate complex is generated in situ in the early stages of the reaction. Therefore, a metal oleate complex seems to be an ideal precursor for the synthesis of monodisperse nanocrystals.[16] Detailed studies on the formation mechanism of MnO nanoparticles by heating a manganese stearate complex in high boiling solvents have been accomplished by Chen et al.[17]

Here we report the synthesis of MnO nanoparticles by a related method[16,18] using the decomposition of a manganese oleate complex at high temperatures in high-boiling-point solvents. We were able to produce MnO nanocrystals with high crystallinity and exceptionally narrow size distribution (in some cases with $\sigma < 3\%$). In addition, we observed that the heating rate has a major influence on the dispersity of the final product.

Experimental Section

All reactions were carried out using standard Schlenk conditions. All syntheses were carried out in a home-built metal bath heater equipped with a temperature control and monitoring unit. The heater was made out of brass and equipped with two 180 W heating elements operating at 220 V and a Pt100 temperature sensor. It was filled with 1.2 kg of Wood metal (Roth, $T_M = 70$ °C).

All syntheses were carried out under argon and using commercially available reagents: 1-tetradecene (technical grade, 92%, Aldrich), 1-hexadecene (technical grade, 92%, Aldrich), 1-octadecene (technical grade, 90%, ACROS), tri-n-octylamine (98%, Fluka), oleic acid (technical grade, Fisher), methanol, hexane, acetone, ethanol, and manganese chloride tetrahydrate ($MnCl_2 \times 4H_2O$, 99%, Aldrich) were used as received.

Synthesis of the Manganese Oleate Precursor. Manganese oleate was prepared according to a reported procedure[16] with some modifications: 7.94 g (40 mmol) of manganese chloride tetrahydrate and 22.60 g (80 mmol) oleic acid were dissolved in 200 mL of methanol. A solution of 3.2 g (80 mmol) of sodium hydroxide in 200 mL of methanol was added dropwise to the stirred Mn-/oleic acid solution over a period of 1 h. The initially clear colorless mixture turned pink, and a deep red oily substance precipitated. After being stirred for another hour, the solvent was discarded and the product washed with water, ethanol, and acetone. The oily residue was dissolved in hexane and dried over $MgSO_4$. After evaporating the solvent the product was dried in vacuo (1×10^{-2} mbar) at 100−150 °C for 2 h to produce a deep red waxy solid.

Synthesis of MnO Nanoparticles. In a typical reaction, 1.24 g (2 mmol) of the manganese oleate were dissolved in 10 g of solvent and degassed at 70 °C in vacuo (1×10^{-2} mbar) for 2 h and intermittently backfilled with argon to remove any moisture and oxygen. The reaction mixture was subsequently treated with a definitive temperature program. First of all the solution was rapidly heated to 200 °C with approximately 5 °C/min. For the further course of the reaction the heating rate was fixed to 1.5 °C/min and the temperature was held at reflux (318 °C) for 1 h. The as-prepared nanocrystals were easily soluble in nonpolar solvents such as hexane or toluene. The nanoparticles were washed three times according to the following procedure: They were first dissolved in hexane, precipitated with acetone or ethanol, and subsequently collected by centrifugation. The washed nanoparticles were thereupon redissolved in hexane or toluene for storage. Depending on solvent, reaction time, temperature, and heating, rate different particle sizes and shapes were obtained.

Nanoparticle Characterization. The particles were characterized by means of powder X-ray diffraction (XRD), transmission electron microscopy (TEM), Fourier transformed infrared spectroscopy (FT-IR), atomic absorption spectroscopy (AAS), nuclear magnetic resonance spectroscopy (NMR), thermogravimetric analysis (TGA), and X-ray photoelectron spectroscopy (XPS). The magnetic properties of the MnO nanoparticles were investigated with a superconducting quantum interference device (SQUID). XRD measurements were performed on a Bruker D8 Advance diffractometer equipped with a Sol-X energy-dispersive detector and operating with Mo Kα radiation. Full pattern profile fits were performed with TOPAS Academic V1.0 applying the fundamental parameter approach.[19] Samples for transmission electron microscopy were prepared by placing a drop of dilute nanoparticle solution in hexane on a carbon coated copper grid. Low-resolution TEM images and ED patterns were recorded on a Philips EM420 microscope operating at an acceleration voltage of 120 kV. High-resolution TEM data was obtained on a FEI Tecnai F30 S-TWIN with a 300 kV field emission gun. FT-IR spectra were acquired on a Nicolet 5DXC spectrometer. For AAS measurements ethanol was added to each sample to precipitate any nanoparticles. After centrifugation the supernatant was treated with conc. HNO_3 to oxidize all organic components. Magnetic measurements were carried out using a Quantum Design MPMS-XL SQUID magnetometer. Experimental data were corrected for diamagnetism using Pascal's constants.[20] XPS data were acquired on a VG ECA-LAB MK2. AAS experiments were performed on a Perkin-Elmer 5100 ZL.

Results and Discussion

X-ray diffraction data were acquired in order to characterize phase purity of the final product (see Figure 1). Particle sizes were estimated by deconvolution of the peak-broadening within the framework of the fundamental parameter approach; they are in good agreement with the values obtained from TEM analysis (average values from approximately 200 individual particles). The observed intensities match well with the cubic rock-salt structure of MnO (*cF*8, $Fm\bar{3}m$); no secondary phases were detected.

Thermal Decomposition of Manganese Oleate. As the MnO particles are formed by thermal decomposition of the manganese oleate precursor, thermogravimetric analysis was performed to examine its decomposition behavior. Usually, metal carboxylates decompose at temperatures around 300 °C, and it is known that this process is accompanied by the formation of free radicals.[21] These radicals can undergo various reactions such as recombination, decay into smaller fragments, or−as

(16) Park, J.; Joo, J.; Kwon, S. G.; Jang, Y.; Hyeon, T. *Angew. Chem., Int. Ed.* **2007**, *46*, 4630–4660.
(17) Chen, Y.; Johnson, E.; Peng, X. *J. Am. Chem. Soc.* **2007**, *129*, 10937–10947.
(18) Jana, N. R.; Chen, Y.; Peng, X. *Chem. Mater.* **2004**, *16*, 3931–3935.
(19) Cheary, R. W.; Coelho, A.; J. Appl. Crystallogr. **1992**, *25*, 109. Coelho, A. TOPAS Academic, V1.0; **2004**.
(20) Haberditzl, W. Magnetochemie; Akademie-Verlag: Berlin, 1968.
(21) Kwon, G. S.; Piao, Y.; Park, J.; Angappane, S.; Jo, Y.; Hwang, N. M.; Park, J. G.; Hyeon, T. *J. Am. Chem. Soc.* **2007**, *129*, 12571–12584.

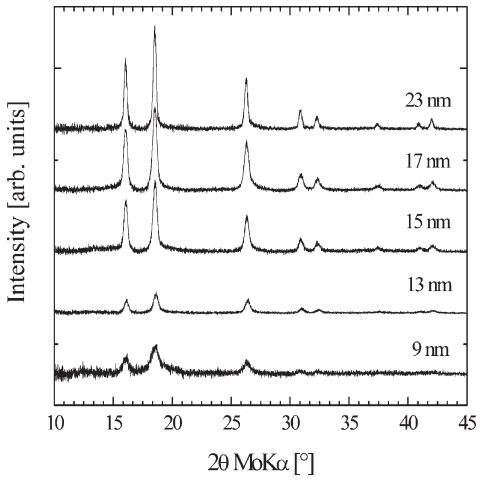

Figure 1. Size-dependent powder XRD patterns of MnO nanoparticle samples.

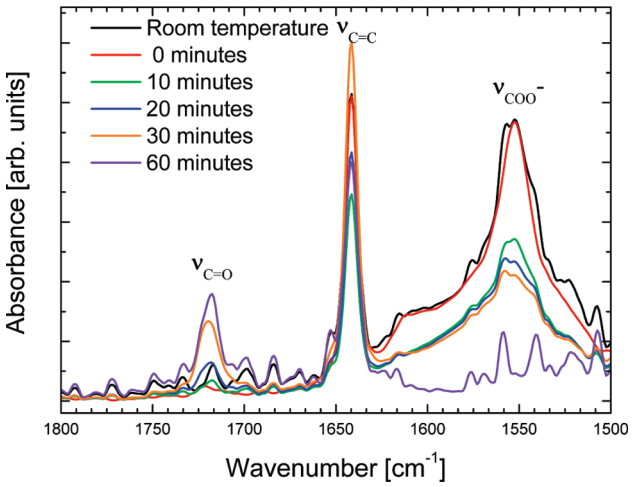

Figure 2. FT-IR spectra of aliquots taken at different stages of the reaction after the reaction solution had reached 200 °C (the variation of intensity of the C=C band at 1645 cm^{-1} is due to varying amounts of solvent in the samples).

desired here—propagate the decomposition by reacting with other carboxylate complexes. As a result, a variety of compounds are formed, including CO, CO_2, free acids, ketones, hydrocarbons, and of course, metal oxide target compounds. However, a detailed and stoichiometric description of this process has not yet been established.

Figure S1 (see the Supporting Information) shows the thermogravimetric traces (in Ar) of manganese oleate. The first step in the diagram can be associated with a mass loss that we ascribe to two molecules of CO_2 (Δm_{rel} = 14.5% ± 0.5% loss corresponding to a molar mass of 89.5 g mol^{-1} ± 3.1 g mol^{-1}). This decomposition is initiated between 220 and 230 °C. Around 400 °C, there is a sharper fall in mass that corresponds to the remaining organic residues being stripped off (Δm_{rel} = 74.2% ± 0.5% mass loss). The remaining solid material (Δm_{rel} = 11.4% ± 0.5% of the starting material) with a mass of 70.4 g mol^{-1} ± 3.1 g mol^{-1} corresponds in good approximation to MnO (molar mass 70.94 g mol^{-1}).

Nucleation and Growth. A detailed understanding of the nucleation and growth process is essential for the controlled synthesis of monodisperse MnO nanoparticles. Unfortunately, an observation of the nucleation event by common techniques is very difficult. We have used FT-IR spectroscopy, TEM, and AAS analysis to study the decomposition of the precursor and to evaluate the mechanism of the MnO particle formation.

After having reached 200 °C, the reaction mixture was heated with a constant heating rate of 1.5 °C/min and aliquots of the solution were taken at different times and temperatures. Figure 2 shows FT-IR spectra of these samples. Typical TEM images of the resulting nanoparticles at different stages of the synthesis are presented in Figure 3. At room temperature, the antisymmetric stretching vibration of the oleate group is clearly detectable at 1555 cm^{-1}. At temperatures above 200 °C, the color of the solution changed from light red to brown. Nevertheless, neither a significant depletion of precursor nor nanocrystals were detectable. As the temperature increases, the oleate complex starts decomposing, as concluded from the reduced intensities of the $RCOO^-$

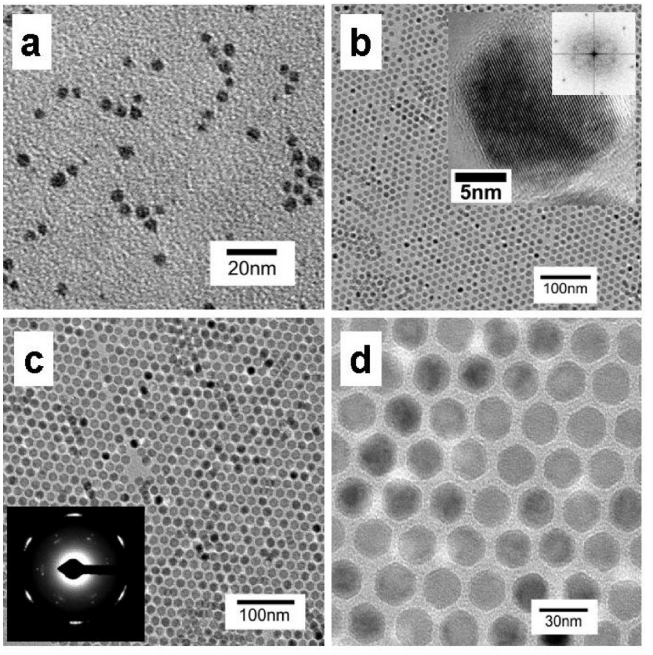

Figure 3. TEM images of MnO nanoparticles at different stages of the reaction. Nanoparticles isolated (a) immediately after initiated precursor decomposition, (b) after ~2.5 min, (c) after 60 min of reflux in 1-hexadecene, (d) after 60 min of reflux in 1-octadecene. Inset (b) HR-TEM and FFT image of a single particle. Inset (c) SAED image corresponding to image (c).

bands of the samples heated at 215 °C (10 min in Figure 3) and 230 °C (20 min in Figure 2). In accordance with earlier observations,[17] we assume that during this decomposition process, free oleic acid and small MnO clusters are formed. This assumption is confirmed by the fact that an absorption band appears at 1719 cm^{-1} in the spectra, which can be assigned to the carbonyl stretching mode of free oleic acid (see Figure 2). We expect that in the further course of the reaction, the concentration of these MnO clusters increases until a critical value of supersaturation is reached upon which spontaneous nucleation is initiated. Consequently, the MnO cluster concentration

decreases rapidly below a level where the net nucleation rate is zero; this is in agreement with the concept proposed by LaMer.[10]

Figure 3a shows nanoparticles isolated in these early stages of the reaction. They are poorly crystalline with an average diameter of 4.5 nm and a relatively broad size distribution. Growth is very fast during this phase of the reaction, because in samples taken shortly afterward (Figure 3b, ~2.5 min after taking the first sample (230 °C)) the particles have not only grown to a diameter of 8.5 nm but also appear more uniform in size. Subsequently the nanocrystals grow further by consuming precursor molecules from solution without any new nuclei being formed.

Because all particles emerge virtually at the same time, their growth histories are nearly identical and remain independent from the nucleation event. Therefore, their size distribution is exceptionally narrow with standard deviation values below 5%. This concept has often been used to describe the formation of monodisperse nanoparticles in the past and is generally referred to as "separation of nucleation and growth" mechanism.[21−23] In contrast to the results presented by Chen et al.[17] for the manganese stearate method, the oleate precursor was still detectable in the reaction solution by FT-IR spectroscopy and AAS even at higher temperatures and after prolonged reaction times (see Figures 2 and 4). This fact indicates that the growth of the nanocrystals occurs by consumption of the dissolved precursor.

Above 250 °C, a light greenish precipitate appears that turns dark green at higher temperatures and redissolves again at approximately 300 °C, forming a clear green solution. After 60 min of reaction, the carboxylate band at 1555 cm^{-1} (Figure 2) has almost disappeared completely. The remaining intensity can be attributed to the carboxylate band of the oleate molecules which cover the surfaces of the nanoparticles. The carbonyl band at 1719 cm^{-1}, on the other hand, shows strong absorbance, which suggests a nearly complete conversion of the precursor. This is in agreement with the depletion of the concentration of free Mn^{2+} as obtained from AAS measurements (Figure 4). As a consequence, no further growth of the nanoparticles under consumption of dissolved manganese oleate is possible. Images c and d in Figure 3 show particles isolated after 60 min of reflux from reaction solutions containing 1-hexadecene and 1-octadecene, respectively. They have average diameters of 17 and 22.5 nm, respectively.

The evolution of particle size with time was studied to derive the kinetics of the MnO nanoparticle formation (see Figure 4). As mentioned above the size of the nanocrystals increases rapidly within the first minutes of reaction. After 30 min their growth slows down and eventually stagnates in the further course of the experiment. The AAS results confirm a rapid conversion of the

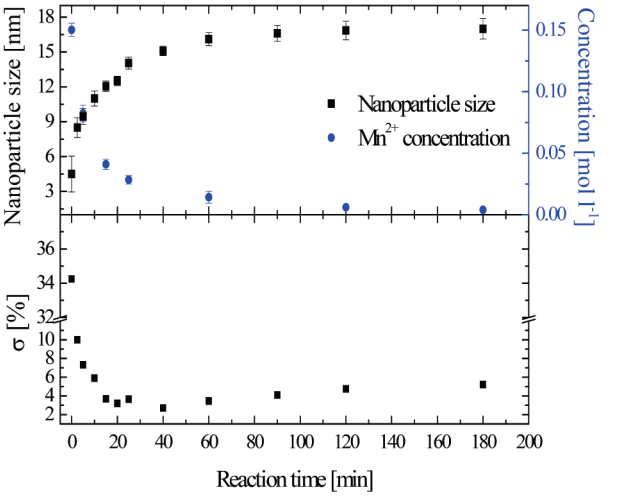

Figure 4. Evolution of particle size and concentration of free Mn^{2+} with reaction time in 1-hexadecene (top), evolution of the standard deviation of the mean particle diameter with time (bottom).

precursor in the initial phase of the experiment. However, manganese oleate is still detectable as Mn^{2+} in the solution even after 60 min and longer, suggesting once more that particle growth is driven by a consumption of dissolved precursor molecules. The observed depletion of the manganese precursor matches well with the growth of the particles with time. Figure 4 (bottom) shows the evolution of the relative standard deviation of the particles size as a function of time. A decrease of σ from 34.2 to 7.3% within 5 min indicates a fast focusing of the size distribution. The standard deviation reaches a minimum value of 2.7% after 40 min. Surprisingly, neither a significant broadening of the size distribution, nor changes in size or shape of the particles occurred even after the reaction was continued for 180 min. This behavior is atypical for a classical Ostwald ripening process.

Figure 5 shows the evolution of particle size as a function of reaction temperature. The crystal size increases almost linearly with temperature for all solvents used. However, a correlation between size and solvent becomes apparent when the particle sizes at a fixed reaction temperature of 250 °C are compared. When the reaction is heated to 250 °C in 1-octadecene (C_{18}, bp. 318 °C), the nanoparticles grow to a mean diameter of 14.6 nm (σ = 9.7%), whereas in 1-hexadecene (C_{16}, bp. 275 °C) and 1-tetradecene (C_{14}, bp. 254 °C), they grow up only to 13.3 nm (σ = 5.4%) and 12.1 nm (σ = 4.4%), respectively, at this temperature. It also seems that the narrowest size distributions are achieved in the lower boiling solvents 1-hexadecene and 1-tetradecene.

When trioctylamine (TOA) was used as a solvent, however, the results are significantly different. Figure 6 shows TEM micrographs of particles synthesized in TOA. The particles appear randomly shaped, forming multipods and rods. At the beginning of the reaction, the crystals are well-faceted with sharp edges. As the reaction proceeds, the edges are smoothed out and the particles lose their shape. This result is consistent with

(22) Peng, X.; Wickham, J.; Alivisatos, A. P. *J. Am. Chem. Soc.* **1998**, *120*, 5343–5344.
(23) Peng, Z. A.; Peng, X. *J. Am. Chem. Soc.* **2002**, *124*, 3343–3353.

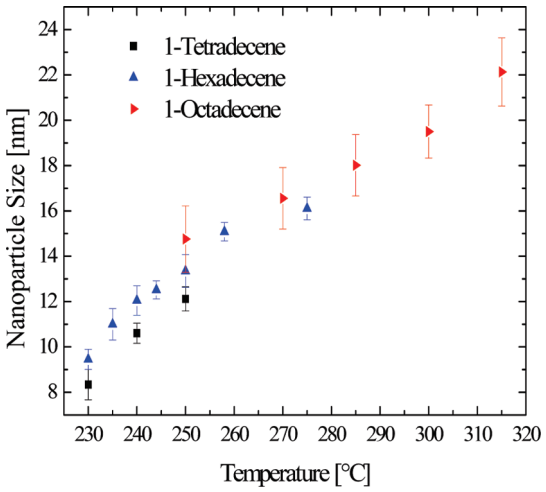

Figure 5. MnO nanoparticle size as a function of temperature and solvent.

observations reported by Ould-Ely et al.[24] who synthesized MnO nanocrystals by decomposition of manganese formate in a mixture of oleic acid and trioctylamine. The reason for this behavior is presumably that TOA itself, different from long-chained alkenes, has a strong affinity to the surface of metal oxides.[25] It has often been used as stabilizing agent in the synthesis of nanoparticles.[13] Therefore, a competition reaction on the nanocrystal surface between the surface ligands oleate and TOA seems likely that results in an additional growth on partly uncovered surfaces of the crystals.

An interesting feature of the present system emerges when the solution is cooled to room temperature after reaction was complete. Below 250 °C, the initially clear green mixture turns brown, and below 200 °C, it turns dark brown while remaining clear. However, the color changes to green again when the mixture is reheated above 280 °C. This thermochromic effect can be repeated several times.

Surface Ligands of the Nanoparticles. A key aspect in the synthesis of nanoparticles is to overcome the high surface energy and to stabilize their thermodynamically unfavorable state. In most synthetic methods, this task is accomplished by adding certain organic molecules that are able to bind onto the surface of the crystals and stabilize them against aggregation and oxidation. These stabilizing agents also control nucleation and growth and often comprise long-chain phosphines such as trioctylphosphine, long-chain thiols, or fatty acids like stearic acid or oleic acid.

We used different techniques to determine the coordination of the surfactant molecules (oleic acid) on the surface of the nanoparticles. Figure 7a shows the FT-IR spectra of oleic acid, manganese oleate, and washed MnO

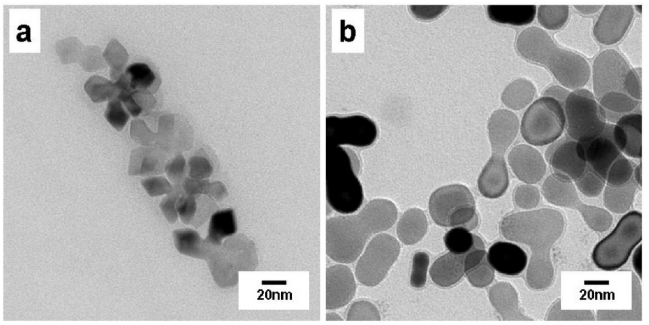

Figure 6. TEM images of MnO nanoparticles prepared in trioctylamine after (a) 5 and (b) 60 min.

nanocrystals. The characteristic bands of the oleyl group are present in all spectra. The weak absorption band at 2956 cm^{-1} results from the asymmetric CH_3 stretching mode. Two bands at 2922 and 2852 cm^{-1} can be assigned to the symmetric and asymmetric CH_2-stretching modes, respectively. Additionally, a small maximum at 3005 cm^{-1}, due to asymmetric stretching of the vinyl C−H bond, is also characteristic for the oleyl group. The free carbonyl stretching mode of the acid is visible at 1711 cm^{-1}. In comparison, the intensity of this band is reduced in the other samples, and strong absorption bands that can be assigned to the asymmetric and symmetric stretching bands of the $RCOO^-$ group, respectively, appear at 1555 and 1410 cm^{-1}. Furthermore, the difference of 145 cm^{-1} between both stretching modes is characteristic for a bidentate coordination of the carboxylate to a metal atom, as has been observed in zinc oleate complexes.[26,27] Maxima at 1462, 1410, 1379, and 1286 cm^{-1} in the oleic acid spectrum can be assigned to deformation vibrations of CH_2 and CH_3 groups of the alkyl chain whereas the broad absorption band at 930 cm^{-1} can be ascribed to the O−H···O bending vibration of the carboxylic acid group. In a simplistic view, spherical MnO nanoparticles are terminated by facets whose structure contains fragments of the polar (111) surface. In contrast to nonpolar (100) surfaces of rocksalt structured metal oxides, which are thermodynamically stable, (111) polar surfaces of bulk single crystal oxides are unstable if they remain in the bulk terminated structure because of the diverging surface potential.[27] From a theoretical point of view, it has been shown for crystalline surfaces that the compensation of polarity occurs through an interplay of different mechanisms, such as changes in the surface electronic structure, structural reconstructions accompanied by changes in the surface stoichiometry, and interaction with the residual atmosphere adsorption, hydroxylation, etc.[29] Thus, the stabilization

(24) (a) Ould-Ely, T.; Prieto-Centurion, D.; Kumar, A.; Guo, W.; Knowles, W. V.; Asokan, S.; Wong, M. S.; Rusakova, I.; Lüttge, A.; Whitmire, K. H. *Chem. Mater.* **2006**, *18*, 1821–1829. (b) Rusakova, I.; Ould-Ely, T.; Hofmann, C.; Prieto-Centurin, D.; Levin, C. S.; Halas, N. J.; Lüttge, A.; Whitmire, K. H. *Chem. Mater.* **2007**, *19*, 1369–1375.
(25) Ritchie, J. E.; Murray, W. E.; Kershan, K.; Diaz, V.; Tran, L.; McDevitt, J. T. *J. Am. Chem. Soc.* **1999**, *121*, 7447–7448.
(26) Barman, S.; Vasudevan, S. *J. Phys. Chem. B* **2007**, *111*, 5212–5217.
(27) Alcock, N. W.; Tracy, V. M.; Waddington, T. C. *J. Chem. Soc., Dalton Trans.* **1976**, 2243–2246.
(28) Wolf, D. *Phys. Rev. Lett.* **1992**, *68*, 3315–3318.
(29) (a) Langell, M. A.; Berie, C. L.; Nassir, M. H.; Wulser, K. W. *Surf. Sci.* **1994**, *320*, 25–38. (b) Dulub, O.; Diebold, U.; Kresse, G. *Phys. Rev. Lett.* **2003**, *90*, 016102/1–4. (c) Kresse, G.; Dulub, O.; Diebold, U. *Phys. Rev. B* **2003**, *68*, 245409/1–15. (d) Lazarov, V. K.; Plass, R.; Poon, H. C.; Saldin, D. K.; Weinert, M.; Chambers, S. A.; Gajdardziska-Josifovska, M. M. *Phys. Rev. B* **2005**, *71*, 115434/1–9.

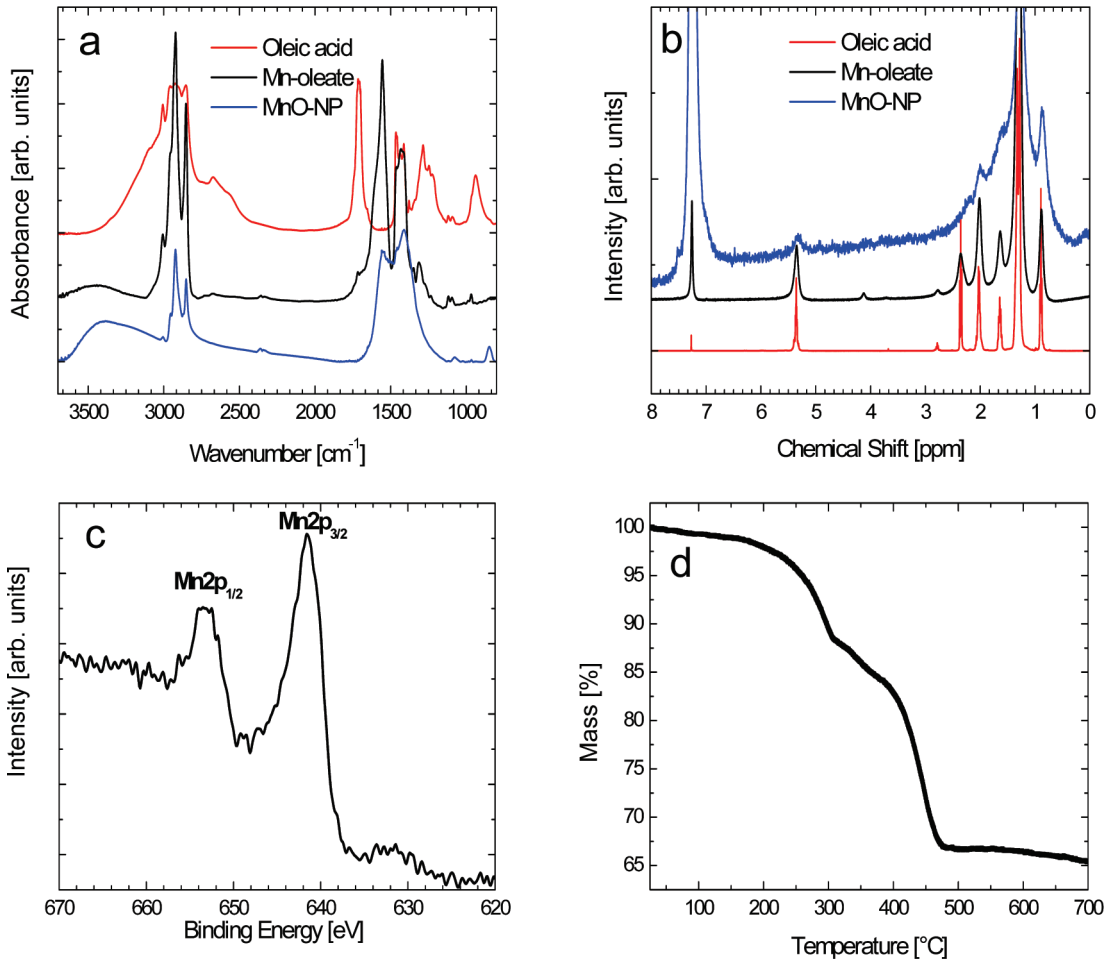

Figure 7. (a) FT-IR spectra of oleic acid, manganese oleate, and washed MnO nanoparticles (to remove excess surfactants and any byproducts of the reaction. Therefore, the strong absorption bands at 1555 and 1410 cm^{-1} are due to the asymmetric and symmetric stretching modes of the carboxylate group of the oleate molecules covering the surface). (b) ^{1}H NMR spectra of oleic acid, manganese oleate, and washed MnO nanoparticles. (c) High-resolution XPS scans of the Mn 2p region. (d) TGA curve of washed MnO nanocrystals (∅ = 8.5 nm).

of spherical nanoparticles by the charged carboxylate ligands is compatible with a binding of the ligands to the polar (111) surface. On the other hand, the uncharged amine ligand cannot stabilize the MnO (111) surface sufficiently, and particles terminated by the MnO(100) surface are formed. The presence of the very weak carbonyl peak at 1710 cm^{-1} suggests the presence of trace amounts of free oleic acid in the manganese oleate complex. However, in the MnO-NP sample, no free oleic acid is detectable.

Nuclear magnetic resonance (NMR) spectroscopy is typically used to determine the coordination and interactions of ligands on the surface of diamagnetic nanoparticles.[30,31] NMR spectroscopy of paramagnetic nanocrystals is only rarely reported due to large broadening effects caused by the large magnetic moment of paramagnetic materials.[32,33] Figure 7b compares the ^{1}H NMR spectra of free oleic acid, the manganese oleate complex and washed MnO-NP. The signal broadening is clearly visible in the MnO-NP sample, which complicates a spectral assignment. Willis et al.[32] reported a reduction of the double bond of oleic acid at high reaction temperatures (350 °C) during the synthesis of iron oxide nanoparticles. Nevertheless, the vinyl and allyl proton resonances appear at 5.34 and 2.01 ppm in all three samples, suggesting that no loss of unsaturation (hydration of the double bond) occurs during the synthesis. This is presumably due to the relatively low reaction temperatures used in our synthesis.

Further characterization of the ligand-coated MnO nanocrystals was performed using high-resolution XPS. Renaud and Barbier[34] reported that the MnO (111) single-crystal surface is nonstoichiometric, containing a mixture of the MnO (111) and Mn_3O_4 (111) phases; the latter
was suggested to play a stabilizing role in compensating the polarity. Figure 7c shows a high-resolution XPS spectrum of the Mn 2p region acquired on a MnO nanoparticle sample that was washed and stored in air

(30) Sachleben, J. R.; Colvin, V.; Emsley, L.; Wooten, E. W.; Alivisatos, A. P. *J. Phys. Chem. B* **1998**, *102*, 10117–10128.
(31) Ladizhansky, V.; Hodes, G.; Vega, S. *J. Phys. Chem. B* **1998**, *102*, 8505–8509.
(32) Willis, A. L.; Turro, N. J.; O'Brien, S. *Chem. Mater.* **2005**, *17*, 5970–5975.
(33) Benn, R.; Rufinska, A. *Angew. Chem., Int. Ed.* **1986**, *25*, 861–881.
(34) (a) Renaud, G.; Barbier, A. The Chemical Physics of Solid Surfaces; Elsevier: New York, 2001; Vol. *9*, p 256. (b) Heinrich, V. E.; Cox, P. A. The Surface Science of Metal Oxides; Cambridge University Press: Cambridge, U.K., 1994; pp 353−355.

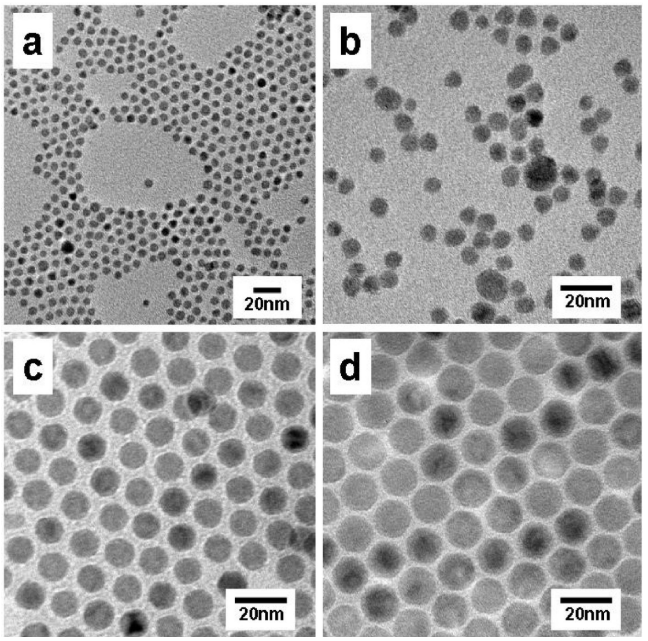

Figure 8. TEM images of MnO nanoparticles synthesized at different heating rates: (a) 90 , (b) 50, (c) 3.3, and (d) 1.5 °C min^{-1}.

for several days. The Mn $2p_{1/2}$ and $2p_{3/2}$ signals are located at 653.4 and 641.4 eV, respectively. These values are in good agreement with literature values of Mn^{2+} in bulk MnO.[35,36] These results confirm, within the limit of detection, that no significant oxidation of Mn^{2+} to Mn^{3+} on the surface of the nanoparticles occurred during the reaction and the subsequent purification and indicates the importance of surface coverage with the oleate ligand. However, it should be stated that a high-resolution electron energy loss (HREEL) spectrum is more sensitive than XPS in detecting cation surface defects leading to the formation of overlayers from higher oxides such as Mn_2O_3 or Mn_3O_4.[37] Finally, the amount of oleate on the nanoparticle surface was determined by thermogravimetric analysis. A typical TGA trace for MnO nanoparticles with 8.5 nm diameter is presented in Figure 7d. The first step can again be associated to loss of CO_2. The second step in the diagram is due to decomposition of the remaining organic residues. The oleate on the surface sums up to a fraction $\Delta m_{rel} = 34\% \pm 0.5\%$ of the total mass.

Influence of the Heating Rate. It was found that the heating rate had a major influence not only on the size, but also on the dispersity of the nanoparticles. Images of nanocrystals synthesized with different heating rates are displayed in Figure 8. All images show particles formed in reaction mixtures heated to 300 °C in 1-octadecene solvent after 1 h of aging. It appears that the particle size is inversely dependent on the heating rate, whereas the size distribution is narrowest when the reaction

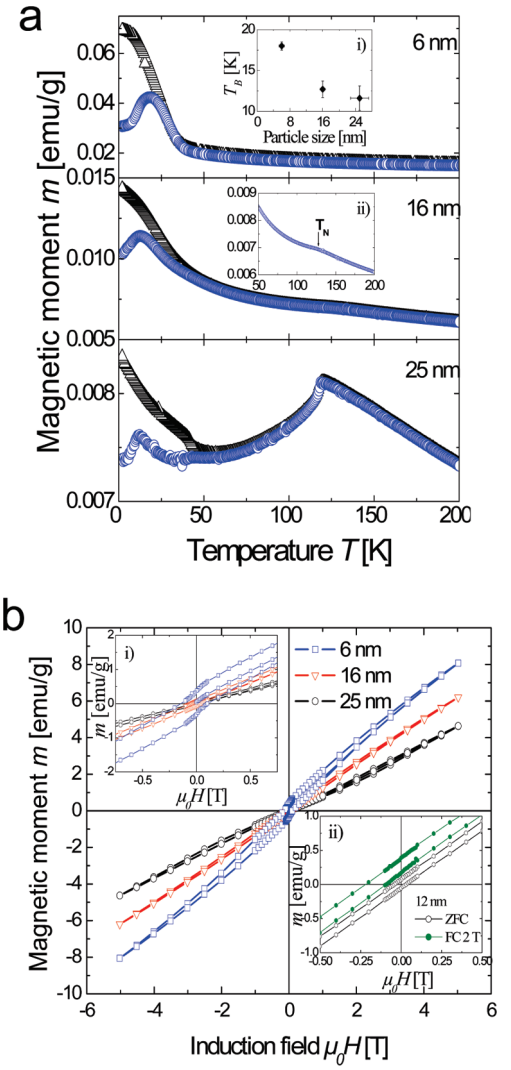

Figure 9. (a) Size-dependent ZFC (blue circles) and FC (black triangles) magnetization measurements of MnO nanoparticles in an applied field of 100 Oe. Inset (i) displays the size dependency of T_B, inset (ii) shows the temperature range from 50 to 200 K of the 16 nm particles on an enlarged scale. (b) Hysteresis loops of different-sized MnO nanoparticles measured at 5 K. Inset (i) shows enlarged view of the hysteresis loops. Inset (ii) shows hysteresis loops of 12 nm particles measured in a ZFC and a FC (2 T) state.

solution is heated slowly. In Figure 8a (90 °C/min), the particles have an average diameter of 6.5 nm ($\sigma = 12.5\%$), in Figure 8b (50 °C/min) the particle size is 8.5 nm ($\sigma = 19.3\%$). When slow heating rates are used, the nanocrystals appear more uniform in size and shape, as can be seen in Figure 8c (3.3 °C/min) with $d = 12.5$ nm ($\sigma = 5.3\%$) and Figure 8d (1.5 °C/min) with $d = 18.9$ nm ($\sigma = 5.5\%$).

Magnetic Properties. It has been reported that MnO nanoparticles show weak ferromagnetic behavior at low temperatures although bulk MnO is antiferromagnetic with $T_N = 122$.[38] The observed weak ferromagnetism was explained by the existence of noncompensated surface spins of the antiferromagnetic core of the MnO nanoparticle. These disordered spins originate from a change in the metal coordination at the surface.[39]

(35) Tan, B. J.; Klabunde, K. J.; Sherwood, P. M. A. *J. Am. Chem. Soc.* **1991**, *113*, 855–861.
(36) Strohmeier, B. R.; Hercules, D. M. *J. Phys. Chem. B* **1984**, *88*, 4922–4929.
(37) Langell, M. A.; Hutchings, C. W.; Carson, G. A.; Nassir, M. H. *J. Vac. Sci. Technol., A* **1996**, *14*, 1956–1961.
(38) Hill, R.; Howard, C. J. *J. Appl. Crystallogr.* **1987**, *20*, 467–476.
(39) Lee, G. H.; Huh, S. H.; Jeong, J. W.; Choi, B. J.; Kim, S. H.; Ri, H.-C. *J. Am. Chem. Soc.* **2002**, *124*, 12094–12095.

Figure 9a shows the field-cooled (FC) and zero-field cooled (ZFC) magnetizations measured in an applied field of 100 Oe, yielding blocking temperatures (T_B) of 18.0, 12.7, and 11.6 K for the 6, 16, and 25 nm particles, respectively. The inverse proportionality of T_B on the size is illustrated in inset a in Figure 9a. Smaller MnO particles exhibit a higher surface-to-volume ratio and thus the higher number of noncompensated surface spins. This leads to a higher blocking temperature and to higher magnetization values compared to larger particles. This result is in good agreement with a results reported by Seo et al.[12] The 16 nm MnO nanoparticles show a weak feature at approximately 122 K, the Néel temperature of bulk MnO (inset b in Figure 9). However, the susceptibility of a MnO antiferromagnetic powder is expected to decrease below T_N. But in the case of the 16 nm particles, a further increase in the susceptibility is observed. The expected behavior is found for the 25 nm particles for which the magnetic transition at T_N is considerably enhanced.

Hysteresis loops at 5 K of different size particles are shown in Figure 9b. An increase in the magnetization and the width of the hysteresis loop with decreasing size is observed. Inset b displays the hysteresis loops of 12 nm MnO particles measured in a ZFC and a FC state with an applied field of 2 T. The exchange coupling between the antiferromagnetic core of the particle and the surface spins leads to a magnetic behavior corresponding to two magnetic systems.[40] This causes a loop shift along the field axis in the FC state. Furthermore, H_C and H_{ex} increase in the field-cooled hysteresis loop. These results demonstrate that the magnetic properties of MnO nanoparticles strongly depend on the size of the particles.

(40) Kodama, R. H.; Berkowitz, A. E.; McNiff, E. J.; Foner, S. *J. Appl. Phys.* **1997**, *81*, 5552–5557.

Summary and Conclusions

In summary, we have shown that MnO nanoparticles can easily be produced by a simple one-pot heating-up method. The nucleation and growth procedure of the particles was studied by TEM, FT-IR, and AAS analysis. Our results suggest a single nucleation event followed by a growth on the existing nuclei. Because nucleation and growth are clearly separated, the crystals grow uniformly, leading to a narrow size distribution. The particle size can be controlled by adjusting the reaction time and temperature, the solvent and the heating rate. The particle size increases with temperature, reaction time, and chain length (boiling point) of the solvent. We investigated the surface of the MnO nanocrystals by FT-IR and NMR and demonstrated that oleate binds to the surface in a bidentate manner. In addition, XPS measurements indicate that no significant oxidation of Mn^{2+} to Mn^{3+} occurred even after several days. Magnetic measurements showed that the magnetic properties strongly depend upon the size of the nanoparticles. Both magnetic moment and blocking temperature increase when the particle size is decreased.

Acknowledgment. This work was supported through the Materials Science Center (MWFZ) and by a grant from the Carl-Zeiss-Stiftung. We thank Siham Ouardi for acquiring the XPS spectra, Dr. Enrico Mugnaioli for HR-TEM measurements, and Dr. Martin Panthöfer for many fruitful discussions.

Supporting Information Available: Thermogravimetric analysis curve of the manganese oleate precursor (PDF). This material is available free of charge via the Internet at http://pubs.acs.org.